Formation of x-ray Newton's rings from nano-scale spallation shells of metals in laser ablation

Masaharu Nishikino,[1,a] Noboru Hasegawa,[1] Takuro Tomita,[2] Yasuo Minami,[3] Takashi Eyama,[2] Naoya Kakimoto,[2] Rui Izutsu,[2] Motoyoshi Baba,[3] Tetsuya Kawachi,[1] and Tohru Suemoto[3]

[1]*Department of Advanced Photon Research, National Institutes for Quantum and Radiological Science and Technology, Kizugawa, Kyoto 619-0215, Japan*
[2]*Faculty of Engineering, Tokushima University, Tokushima 770-8506, Japan*
[3]*Institute for Solid State Physics, The University of Tokyo, Kashiwa-shi, Chiba 277-8581, Japan*

(Received 11 November 2016; accepted 19 January 2017; published online 27 January 2017)

The initial stages of the femtosecond (fs) laser ablation process of gold, platinum, and tungsten were observed by single-shot soft x-ray imaging technique. The formation and evolution of soft x-ray Newton's rings (NRs) were found for the first time. The soft x-ray NRs are caused by the interference between the bulk ablated surface and nanometer-scale thin spallation layer; they originate from the metal surface at pump energy fluence of around 1 J/cm2 and work as a flying soft x-ray beam splitter. [http://dx.doi.org/10.1063/1.4975218]

I. INTRODUCTION

The dynamical processes of laser-induced irreversible phenomena such as laser ablation have been attracting considerable attention for microfabrication (cutting, boring, welding, etc.) using ultra-short laser pulses.[1,2] Femtosecond (fs) laser processing can be applied to micro- and nanometer fabrication of various materials such as metals,[3,4] semiconductors,[5] and insulators.[6] Surface modification such as the formation of periodic grating structures on a metal surface has also been demonstrated under irradiation with multiple fs laser pulses,[7–10] and these structures have been actively studied.[11,12] The observed grating spacing was of the scale of several hundreds of nanometers, and was sometimes shorter than the irradiation laser wavelength. This fs laser ablation process for creating nano-structured surfaces is expected to be used as a novel fabrication technique to modify the wettability,[13] to influence tribological properties,[14,15] to create structural coloring,[16] or to control cell spreading.[17] To realize and improve precision microfabrication techniques using fs laser pulses, a deep understanding of the fundamental processes of laser–matter interaction is important. Several studies on time-resolved imaging of fs laser ablation have been performed using various materials to understand the relevant ablation dynamics.[18–21] During fs laser ablation of metals and semiconductors, transient interference fringes of Newton's rings (NRs) were observed by Sokolowski-Tinten[18–20] using a visible ($\lambda \sim 620$ nm) probe. Refs. 18–20 attribute the NRs to interference between the reflected probe pulses from the thin layer of the spallation shell and the remaining sample surface, as shown in Fig. 1(a).

When the solid sample is excited with an ultra-short pulse laser, a thin film is peeled off by the tensile stress wave and detached from the sample surface.[22–24] This phenomenon is well known as the "spallation" in laser ablation at an irradiation fluence around the ablation threshold.

Assuming a refractive index of unity for the space between the spallation shell and the substrate, the optical path difference between the two reflected beams is defined as $2d \cdot \sin\theta$, as in Fig. 1(b). In a previous experiment,[19] an optical laser was used to probe spallation dynamics. The structure of NRs

[a]Nishikino.masaharu@qst.go.jp

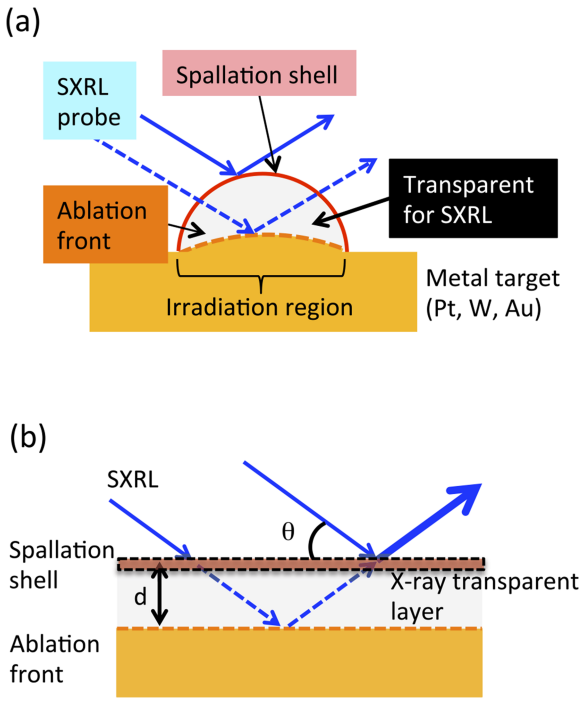

FIG. 1. (a) Schematic view of interference between the reflections from the spallation shell and the ablation front, generating NRs. (b) Interference between two surfaces. In the case of unity refractive index, the path difference between the reflected beams is given by $2d \cdot \sin\theta$. The lateral profiles of the NR images are deduced from the interference condition. For estimation of visibility in Fig. 3(c), the spallation shell is replaced by a slab (a box with broken black lines) with a finite thickness.

resulting from the formation of a dome with the spallation shell is observed at the nanosecond time scale and micrometer depth scale. The optical probe cannot survey regions where the plasma density exceeds the critical density; therefore, the dynamics of fs laser ablation in the very early time stages remain unknown. In contrast to optical light probes, soft x-ray probes have higher spatial resolution due to the 40 times shorter wavelength, and can penetrate and diagnose insides of the high-density electron plasma because the critical density for propagation is proportional to λ^{-2}. Since soft x-rays around 100 eV have the shortest penetration depth for solids and their reflectivity critically depends on the atomic density and roughness of the interface, soft x-rays are the most suitable for observing solid surface morphology.[25–27] In this letter, we report on the pump and probe reflectivity imaging of gold (Au), platinum (Pt), and tungsten (W) surfaces during fs laser ablation using a plasma soft x-ray laser (XRL) as a probe beam. Through the measurement of the temporal evolution of laser ablation using soft x-ray NRs, we found that nanometer spallation metallic shells were working as transient x-ray beam splitters.

II. RESULTS AND DISCUSSION

The x-ray reflection images were observed by the fs-laser pump and XRL probe imaging system.[25–27] The accuracy of fs laser probe timing is less than 3 ps by the real-time monitoring system.[28] The highly coherent soft XRL with a wavelength of 13.9 nm (89.2 eV)[29] was used as probe beam. The output of the XRL beam is sufficient to obtain a x-ray reflection image in a shingle-shot event. The pulse width of the XRL was about 7 ps full width at half maximum (FWHM). The metal samples were 100-nm-thick films evaporated on fused silica substrates. The root mean square initial surface roughness was below 1.0 nm, as measured through atomic force microscopy. The XRL probe beam has a grazing angle of 20° for the ample surface in the experimental setup. The ideal x-ray reflectivity of the XRL probe was 0.36, 0.37, and 0.27 for Au, Pt, and W, respectively.[30] The x-ray reflection image was transferred by a molybdenum/silicon (Mo/Si) multi-layered spherical mirror with magnification factor of 20 and obtained by an x-ray CCD camera. A Ti:Sapphire laser with 80 fs

pulses (FWHM) and a central wavelength of 795 nm was used as pump beam. The linearly polarized pumping laser pulse was focused by a lens onto the sample surface at nearly normal incidence. The irradiation profile had a Gaussian distribution, and the focal spot diameter (FWHM) on the sample surface was about 100 μm. The peak fluence of irradiance was 1.0–1.4 J/cm^2 for all metal samples. The time-evolution of the surface shape was obtained by varying the delay time between the pump fs laser beam and the probe XRL beam with an optical delay stage. The sample was laterally shifted for every shot to get a fresh surface. The temporal resolution of the x-ray imaging system is determined by the length of the soft x-ray pulse. Although the x-ray pulse width is longer than that of the fs pump source, it is high enough to observe an individual laser ablation event. We observed single-shot reflection images with an x-ray CCD camera using an x-ray reflectometer.[26] Figure 2 shows typical soft x-ray images with concentric rings in the fs laser ablation region. Figure 2(a) shows the temporal evolution of the x-ray reflection image of Au at 191, 317, and 607 ps after 1.4 J/cm^2 fs laser irradiation. Figures 2(b) and 2(c) show the x-ray reflection images of Pt at 165 ps after 1.0 J/cm^2 fs laser irradiation and that of W at 148 ps after 1.3 J/cm^2 fs laser irradiation, respectively. All x-ray images in Fig. 2 are about triply expanded in the horizontal direction to compensate for distortion arising from the x-ray grazing incidence. The black hole in the image at t = infinity in (a) corresponds to the crater, where the reflectivity is decreased inside due to the roughness of the ablated surface. In the case of Au, several concentric bright rings appeared inside the dark circular structure of a crater, and the number of concentric rings increased with the delay time from t = 191 to 607 ps, as in Fig. 2(a). The bright rings became narrower toward the edge, and the space between the outer rings was also smaller than that at the central part of the crater until the delay time reached approximately 700 ps. Since these characteristics are very similar to those reported for the Newton's rings in the visible region,[18–20] the observed rings are definitely assigned to Newton's rings, which, to the best of authors′ knowledge, is the first observation in the soft x-ray region. From the pattern of the concentric rings, the spallation shell seemed to have a dome-like structure. Beyond a delay of 700 ps, the concentric rings disappeared, and the dark shadow of the laser-ablated crater finally appeared. In the cases of the Pt and W, we observed also similar concentric rings near the crater edge in a relatively short delay range of 10–20 ps. The short lifetime of NRs in the Pt and W is probably ascribed to the rapid growth of the surface roughness of spallation shells in fs laser ablation.[26] The generation of NRs is supposed to result from the interference between the soft x-rays reflected by the spallation shell and the ablation front behind it, as in Fig. 1. The distance between the two surfaces is obtained from the fringe position of NRs. When the outermost ring is defined as the first ring in the case of a dome structure on the laser-ablated sample surface, the interference condition is calculated as $m\lambda = 2d\cdot\sin\theta$ (m = 1–6), as in Fig. 3(a). Under this condition, a one-period fringe shift corresponded

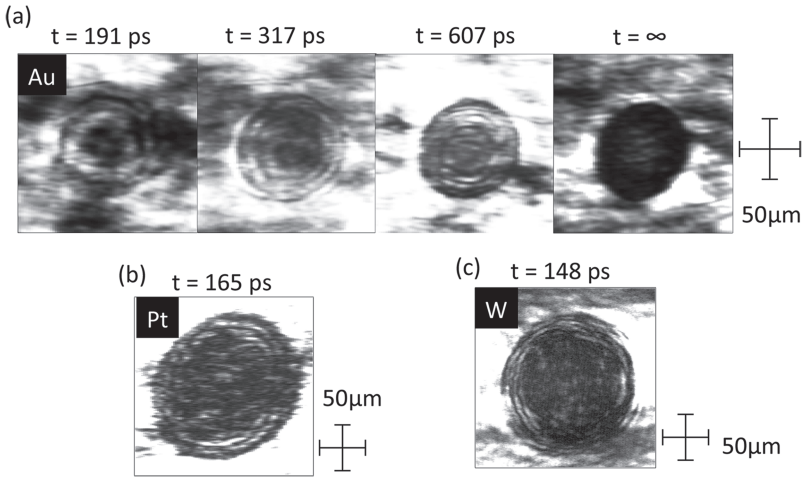

FIG. 2. Soft X-ray Newton's ring image of (a) Au at 191, 317, 607 ps and infinity, (b) Pt at 165 ps, and (c) W at 148 ps after the pump pulse. The contrast has been optimized to better visualize the characteristic features in (a)-(c). The ring structure is recognized in the pattern of the whole image in (a) and near the edge of the ablated holes.

to a height of 20.3 nm for an incident grazing angle of 20°. Figure 3(b) shows the temporal evolution of the estimated lateral profiles of the spallation shell dome as deduced from the NRs together with their quadratic fitting curves. The edges of the quadratic fits are connected to the observed crater edge position at 45 micrometers. The pump beam profile is also shown in Fig. 3(b). The ablation threshold is estimated to be about 0.7 J/cm^2. The spallation speed of the expansion shell at the center position is estimated to be approximately 160 m/s.

To generate NRs, the spallation shell should act as an x-ray beam splitter. In the following, we discuss the properties of the spallation shell from the condition for appearance of NRs. The reflectivity and transmittance of soft x-rays strongly depend on the conditions, such as layer thickness, density, and surface roughness. We model the NR phenomenon in terms of an optical system consisting of the ablation front as a fixed flat surface and the spallation shell as a flying slab with a constant density (see Fig. 1(b)). Some of the x-rays are reflected from the surface of the spallation shell. The transmitted x-rays reflect from the ablation front passing through the spallation shell twice. Figure 3(c) shows the reflectance from the spallation shell and the transmittance of the spallation shell dome at different densities of gold with no roughness. In the case of thin shell dome, almost x-rays transmitted through the spallation shell. Then, the intensity through the spallation dome (dotted line) is determined by the reflection of the ablation front, and becomes near 0.35 for all density cases of the shell. In the case of thick shell dome, no x-rays transmitted through the spallation shell. Then, all x-rays reflected from the spallation shell, and the reflectivity from the spallation shell (solid line) is determined by the reflectivity in each density of the shell. The highest visibility of NRs is realized at the intersection point (indicated by circles) of the reflectivity and the transmittance curves at each density of gold, as seen in Fig. 3(c). The optimum shell thickness is given by the abscissa of the intersection point. In Fig. 2(a), maximum x-ray reflectivity in the unablated area is estimated to be about 30% from the comparison with the x-ray reflection from the flat surface and ablated surface Judging from the noise level of the images, at least 10% reflectance is necessary to distinguish the ring patterns. When the solid's density is 19.3 g/cm^3, the optimum thickness of the spallation shell is 5 nm. When the density is half, the optimum spallation shell thickness is 35 nm. In the lower density condition, both reflectivity and transmittance are always below 10%. For the intersection point to be above the 10%

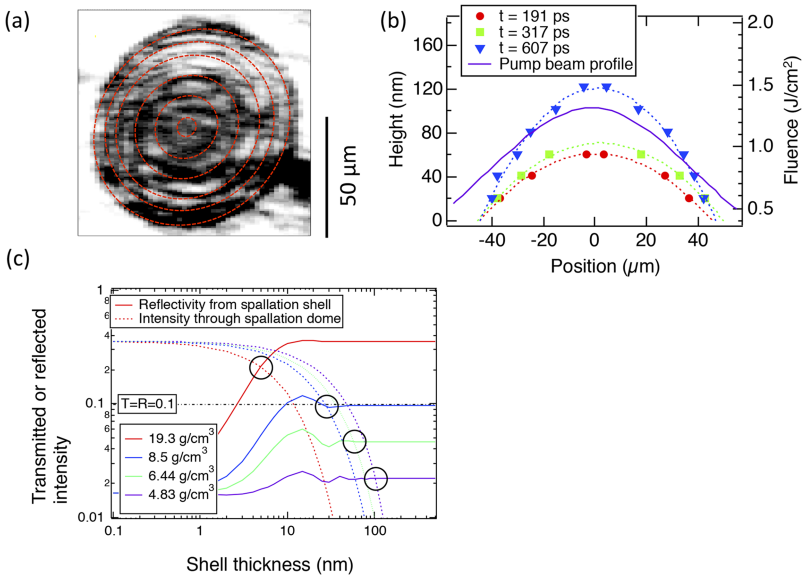

FIG. 3. (a) The concentric rings from the gold sample at t = 607 ps. Six concentric rings are recognized in the pattern as shown by red dotted lines. (b) Estimated spatial distribution of Au at 191, 317, and 607 ps by quadratic fitting of the position of Newton's rings and the distribution of the pump beam fluence. (c) Reflectance from the spallation shell and the transmittance of the spallation shell dome at different densities of solid gold. The intersection points (circles) at each density indicate the combination of density and shell thickness that provide the highest visibility of Newton's rings. The detection threshold of the x-ray intensity is 0.1 (horizontal chained line).

threshold, the density should be larger than 8.5 g/cm^3 and the thickness should lie between 5 and 30 nm. In practice, the reflection (solid lines in Fig. 3(c)) is reduced by the surface roughness and the density gradient. Therefore, the thickness of the shell increases the estimate of other parameters. The surface roughness of both the spallation shell and ablation front should also be under 5 nm to attain a reflectivity of 30% according to the x-ray database.[30]

III. CONCLUSION

In conclusion, we observed direct images of soft x-ray NRs originating from a nanoscale spallation shell dome. Thanks to detailed observations of fs laser ablation and spallation shells, we deduced the mechanism of NR generation, where a very thin, smooth spallation shell that breaks away from the sample surface participates. The understanding of the early stages of laser–matter interaction is important not only from the viewpoint of micromachining of nanoscale structures but also for full time-scale modeling of the relevant molecular dynamics simulations.[31] In addition, the spallation layer seemed to work as a soft x-ray beam splitter and the generation of a transient smooth spallation layer indicates the possibility of fabrication of transient x-ray optics via spatial and temporal dynamic control of the ablating laser pulse.

ACKNOWLEDGMENTS

This work was partly supported by Grant-in Aid for Scientific Research (25286086, 16K05989, and 16K05030) from the Japan Society for the Promotion of Science. The authors are grateful to Dr. Kiminori Kondo of Department of Advanced Photon Research for his help and useful comments. The authors acknowledge the support of the QST X-ray laser staff.

[1] S. K. Sundaram and E. Mazur, Nat. Material **1**, 217 (2002).
[2] R. R. Gattas and E. Mazur, Nat. Photonics **2**, 219 (2008).
[3] F. Korte, J. Koch, and B. N. Chichkov, Appl. Phys. A **79**, 879–881 (2004).
[4] A. Pereira, A. Cros, P. Delaporte, S. Georgiou, A. Ma-nousaki, W. Marine, and M. Sentis, Appl. Phys. A **79**, 1433–1437 (2004).
[5] T.-H. Her, R. J. Finlay, C. Wu, S. Deliwala, and E. Mazur, Appl. Phys. Lett. **73**, 1673–1675 (1998).
[6] F. Korte, J. Serbin, J. Koch, A. Egbert, C. Fallnich, A. Ostendorf, and B. B. Chichkov, Appl. Phys. A **77**, 229–235 (2003).
[7] J. Reif, F. Costache, M. Henyk, and S. V. Pandelov, Appl. Surf. Sci. **197-198**, 891–895 (2002).
[8] N. Yasumaru, K. Miyazaki, and J. Kiuchi, Appl. Phys. A **76**, 983 (2003).
[9] A. Borowiec and H. K. Haugen, Appl. Phys. Lett. **82**, 4462 (2003).
[10] M. Hashida, A. Semerok, O. Govert, G. Petite, Y. Izawa, and J. F-Wagner, Appl. Surf. Sci. **197-198**, 862–867 (2002).
[11] S. Sakabe, M. Hashida, S. Tokita, S. Namba, and K. Okamuro, Phys. Rev. B **79**, 033409 (2009).
[12] G. Miyaji and K. Miyazaki, Opt. Express **16**, 16265 (2008).
[13] B. Wu, M. Zhou, J. Li, X. Ye, G. Li, and L. Cai, Appl. Surf. Sci. **256**, 61–66 (2009).
[14] T. Kato and N. Abe, Rev. Laser Eng. **37**, 510 (2009) (in Japanese).
[15] N. Yasumaru, K. Miyazaki, and J. Kiuchi, Appl Surf. Sci. **254**, 2364 (2008).
[16] A. Vorobyev and C. Guo, Laser Photonics Rev. **7**, 385 (2013).
[17] T. Shinonaga, M. Tsukamoto, T. Kawa, P. Chen, A. Ngai, and T. Hanawa, Appl. Phys. B **119**, 493–496 (2015).
[18] D. von der Linde, K. Sokolowski-Tinten, and J. Bialkowski, Appl. Surf. Sci. **109-110**, 1–10 (1997).
[19] K. Sokolowski-Tinten, J. Bialkowski, A. Cavalleri, D. von der Linde, A. Oparin, J. Meyer-ter-Vehn, and S. I. Anisimov, Phys. Rev. Lett. **81**, 224–227 (1998).
[20] K. Sokolowski-Tinten, J. Bialkowski, A. Cavalleri, and D. von der Linde, Appl. Surf. Sci. **127–129**, 755–760 (1998).
[21] D. von der Linde and K. Sokolowski-Tinten, Appl. Surf. Sci. **54-155**, 1–10 (2000).
[22] S. I. Anisimov, N. A. Inogamov, A. M. Oparin, B. Rethfeld, T. Yabe, M. Ogawa, and V. E. Fortov, Appl. Phys. A **69**, 617–620 (1999).
[23] E. Leveugle, D. S. Ivanov, and L. V. Zhigilei, Appl. Phys. A **79**, 1643–1655 (2004).
[24] C. Wu and L. V. Zhigilei, Appl. Phys. A **114**, 11–32 (2014).
[25] T. Suemoto, K. Terakawa, Y. Ochi, T. Tomita, M. Yamamoto, N. Hasegawa, M. Deki, Y. Minami, and T. Kawachi, Opt. Express **18**, 14114–14122 (2010).
[26] T. Tomita, M. Yamamoto, N. Hasegawa, K. Terakawa, Y. Minami, M. Nishikino, M. Ishino, T. Kaihori, Y. Ochi, T. Kawachi, M. Yamagiwa, and T. Suemoto, Opt. Express **20**, 29329–29337 (2012).
[27] Y. Ochi, K. Terakawa, N. Hasegawa, M. Yamamoto, T. Tomita, T. Kawachi, Y. Minami, M. Nishikino, T. Imazono, M. Ishino, and T. Suemoto, Jpn. J. Appl. Phys. **51** 016601 (2012).
[28] N. Hasegawa, T. Ochi, T. Kawachi, M. Nishikino, M. Ishino, T. Imazono, T. Kaihori, A. Sasaki, K. Terakawa, Y. Minami, T. Tomita, M. Yamamoto, Y. Umeda, M. Yamagiwa, and T. Suemoto, Proc. SPIE **8140**, 81400G (2011).
[29] Y. Ochi, T. Kawachi, N. Hasegawa, M. Nishikino, T. Ohba, M. Tanaka, M. Kishimoto, T. Kaihori, K. Nagashima, and A. Sugiyama, Jpn. J. Appl. Phys. **48**, 120212 (2009).
[30] See http://henke.lbl.gov/optical_contstants/ for The center for x-ray optics, X-Ray Interactions With Matter.
[31] B. J. Demaske, V. V. Zhakhovsky, N. A. Inogamov, and I. I. Oleynik, Phys. Rev. B **82**, 064113 (2010).